SUPPLEMENT TO THE *WELDING JOURNAL*, FEBRUARY 2004
Sponsored by the American Welding Society and the Welding Research Council

An Investigation of Ductility-Dip Cracking in Nickel-Based Weld Metals — Part III

The characteristics of weld-metal grain boundaries associated with elevated-temperature fracture are investigated

M. G. COLLINS, A. J. RAMIREZ, AND J. C. LIPPOLD

ABSTRACT. In Part I of this investigation of ductility-dip cracking (DDC) in nickel-based filler materials, the strain-to-fracture (STF) test (Ref. 1) was used to quantify the DDC susceptibility of two Ni-based filler metals, Filler Metal 52 and Filler Metal 82. Ductility-dip cracking susceptibility was related to the nature of the migrated grain boundaries in these weld metal deposits and the effect of grain boundary "tortuosity" on the mechanical locking of these boundaries at elevated temperature. Part II of this investigation used scanning electron microscopy to examine the DDC fracture surfaces in order to relate fracture mode to temperature, composition, interstitial content (hydrogen), and microstructure. Part III of this investigation uses optical microscopy, high-resolution scanning electron microscopy, and electron backscattered diffraction (EBSD) techniques to further explore the factors that contribute to DDC in Ni-based weld metals. Based on this analysis and the results from Parts I and II of this investigation, a DDC mechanism is described that involves the complex interplay of alloy composition, interstitial and impurity element additions, grain boundary segregation, triple-point grain boundary junctions, grain growth, grain boundary sliding, precipitation, recrystallization, boundary orientation relative to the applied strain, and the contribution of grain boundary misorientation and accumulated local strain. Insight is provided to optimize elevated-temperature ductility in order to avoid DDC in Ni-based weld deposits and other austenitic alloys.

Introduction

From a mechanistic standpoint, relatively little is known or understood about DDC, a solid-state cracking mechanism. Ductility-dip cracking occurs below the effective solidus temperature and separation of grain boundaries has been reported to be characteristic of materials susceptible to DDC (Refs. 2, 3). A number of factors have been reported to contribute to the development of DDC, including specific alloy, impurity, and interstitial element content, segregation, large grain size, grain boundary precipitation, orientation relative to the applied strain, and high levels of weld restraint. The DDC mechanism is still not well understood, nor is the individual effect of these factors. Furthermore, preventive methods for avoiding DDC in highly restrained weldments have proven elusive.

Part I of this investigation (Ref. 4) quantified DDC susceptibility in Filler Metals 52 and 82. Additionally, hydrogen and sulfur additions to the weld metal were evaluated with the STF test and found to increase weld metal DDC susceptibility. Part II of this investigation (Ref. 5) used optical and scanning electron microscopy to study the ductility-dip fracture surfaces, identifying the fracture mode dependence on temperature and microstructure. These two previous studies provided an initial insight into the factors responsible for promoting DDC in highly restrained weld metals. Part III of this investigation uses optical microscopy, high-resolution scanning electron microscopy, and electron backscattered diffraction techniques to further expand on the understanding of the DDC phenomenon. Part III of the investigation has combined the results of the first two parts with the advanced characterization results to provide insight into the mechanism of DDC. The mechanistic aspects of DDC discussed here are thought to apply not only to the Ni-based Filler Metals 52 and 82, but also more broadly to other austenitic alloys, including the austenitic stainless steels.

This investigation has provided further evidence that the Gleeble strain-to-fracture test is an effective, robust test technique for evaluating DDC susceptibility in weld metals. The ability to determine the strain-temperature relationships for DDC as a function of composition has been invaluable for studying elevated-temperature behavior in these alloys.

KEY WORDS

Ductility-Dip Cracking
Nickel-Based Filler Metals
Grain Boundary Characteristics
Strain
Elevated-Temperature Ductility

Experimental Procedures

Advanced characterization was conducted on STF samples of both Filler Metals 52 and 82. The compositions of these filler metals are provided in Table 1. The STF test techniques and test results are reported in Part I (Ref. 4). In this study, grain boundary characteristics of DDC were investigated in more detail than in Part I.

Strain-to-fracture samples were sectioned and mounted in a conductive phenolic powder for advanced characterization using optical and high-resolution scanning electron microscopy, along with X-ray energy-dispersive spectrometry (EDS) and electron backscattered diffraction (EBSD), also known as orientation image microscopy (OIM™). The samples were polished and then electrolytically etched with 10% chromic acid at 2.5 V for 15–20 s. During polishing, an effort was made to minimize material removal, as many cracks were relatively shallow. The polished and etched samples were examined using a Nikon metallograph, and digital photomicrographs were taken with a Hitachi CCD camera. Additionally, a Philips XL-30 field emission gun (FEG) scanning electron microscope (SEM) was

M. G. COLLINS, A. J. RAMIREZ, and J. C. LIPPOLD are with The Ohio State University, Columbus, Ohio.

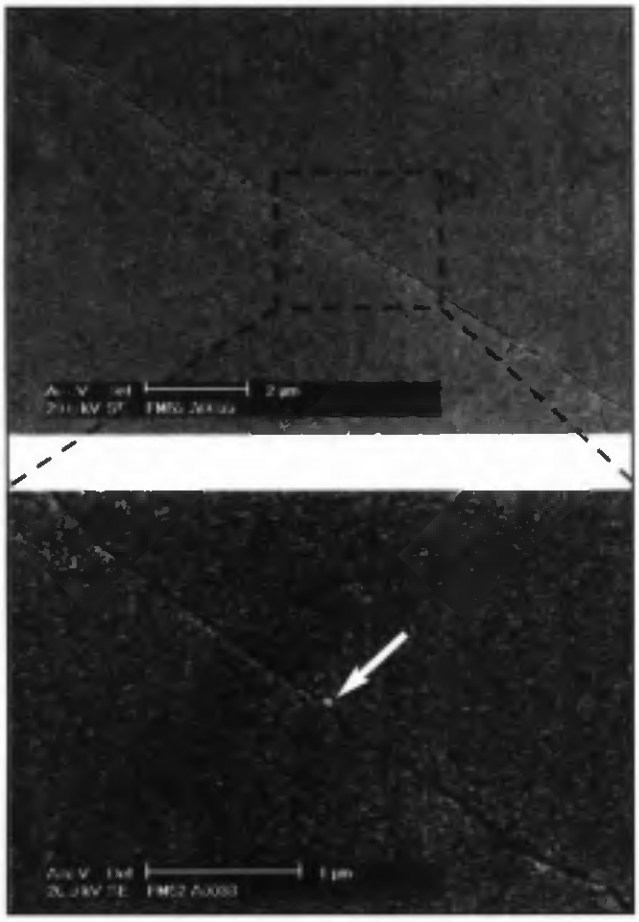

Fig. 1 — Migrated grain boundary in Filler Metal 52 at 986°C and 2.6% strain. (Arrow indicates small particle along boundary.)

Fig. 2 — Precipitation and microsegregation along solidification subgrain boundaries in Filler Metal 52 at 986°C (lower photo reveals boundary migration from "pinning points" at solidification subgrain boundary.)

Table 1 — Chemical Composition of Filler Materials (wt-%)

Element	Filler Metal 52 Heat NX9277	Filler Metal 82 Heat YN6830	Filler Metal 82 Heat YN7355	Filler Metal 82 Heat YB7724
C	0.026	0.04	0.04	0.041
Mn	0.25	2.86	2.75	2.79
Fe	8.88	1.18	0.70	0.90
S	0.0037	0.01	0.002	0.001
Si	0.17	0.12	0.07	0.06
Cu	0.011	0.09	0.07	0.04
Ni	60.12	72.75	72.8	72.98
Al	0.71	N/A	N/A	0.05
Ti	0.50	0.37	0.47	0.45
Cr	29.09	20.1	20.1	19.98
Cb + Ta	0.02	2.3	2.6	2.7
Mo	0.05	N/A	N/A	N/A
P	0.0044	0.007	0.01	0.004
Pb	0.0001	0.004	0.002	0.002
Co		0.05	0.04	0.01

used to analyze the mounted DDC specimens at higher magnifications. The chemical compositions of the precipitates were measured by EDS analysis.

The grain boundary character distribution and local strain distribution were determined on the SEM using EBSD. Electron backscattered diffraction is a widely used technique that collects crystallographic data from a surface with submicron resolution. Because this technique uses the electron beam on an electron microscope, most commonly an SEM, a direct relationship can be established between the microstructure and the crystallographic information (Ref. 6), making it an excellent tool for fracture analysis (Ref. 7). The samples to be used for the EBSD analysis were ground and polished using the same procedure previously described. However, special precautions were taken to minimize the grinding deformation artifacts. After polishing, the samples were lightly electrolytically etched with 10% chromic acid at 1.5 to 2.0 V for 15 s. Electron backscattered diffraction dedicated software, Channel 5™ by HKL Technology, was used for the automated EBSD data acquisition and analysis. The low-angle (1–15 deg) grain boundary distribution was determined based on the EBSD maps. Finally, this low-angle grain boundary information was also used to obtain plastic strain distribution maps in the microstructure (Ref. 8).

Results

Grain Boundary Characterization — SEM

In Part I of this investigation, optical microscopy was used to characterize DDC behavior of Filler Metal 52 and Filler Metal 82. To develop a better understand-

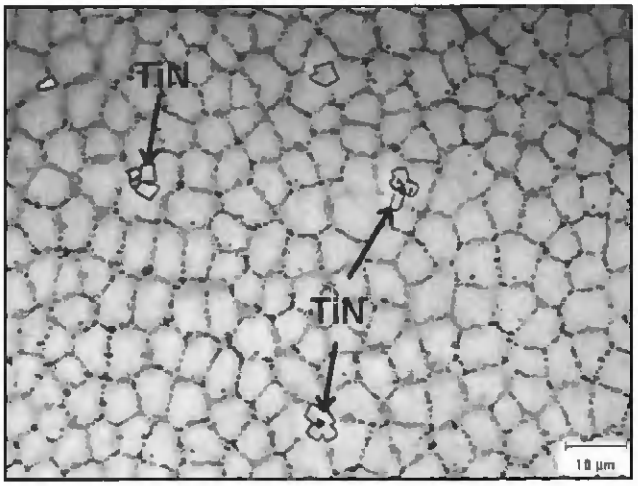

Fig. 3 — Second phases precipitated in the Filler Metal 52 weld metal.

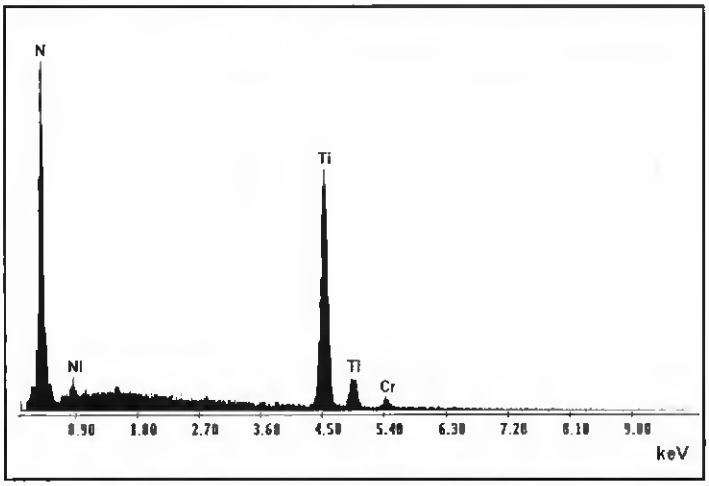

Fig. 4 — Energy-dispersive spectrometry spectra of cuboidal second phases observed in the Filler Metal 52 weld metal.

ing of the factors contributing to DDC, the SEM was used to characterize Filler Metal 52 and Filler Metal 82 grain boundaries at much higher magnifications. It is anticipated that these results, in combination with the metallographic results shown previously in Part I and the fractography analysis presented in Part II of this investigation, would further elucidate the factors contributing to DDC formation.

Filler Metal 52

Migrated grain boundaries in Filler Metal 52 weld deposits exhibit both long/straight and tortuous segments. Under low strain levels, cracking occurred primarily along the straight sections of these boundaries. Examination of the weld-metal microstructure using optical and scanning electron microscopy revealed interdendritic second phases. In addition, clear evidence of grain boundary pinning caused by these interdendritic precipitates was observed. However, these precipitates were not consistently distributed throughout the weld-metal microstructure. Consequently, the regions free of these precipitates underwent more grain boundary migration, resulting in the straight boundaries most susceptible to DDC. Figure 1 illustrates a long, straight migrated grain boundary in a Filler Metal 52 multipass weld. Both the boundary and the microstructure clearly lack any impediments (precipitates or second phases) to "lock" the boundary in place, or to "pin" boundary movement, resulting in uninhibited boundary migration and the consequent grain boundary straightening, grain growth, and increased susceptibility to DDC.

Figure 2 clearly reveals solidification subgrain boundaries, migrated grain boundaries, and DDC along migrated grain boundaries. The solidification subgrain boundaries exhibit both segregation (as revealed by the contrast) and two different types of precipitates, shown in Fig. 3. The large precipitates are cuboidal TiN particles, approximately 5 µm in their largest dimension. Figure 4 shows a typical EDS spectrum for this precipitate, indicating that Ti and N are essentially the only elements present. The small Cr and Ni peaks probably reflect the surrounding matrix. The size and location of these large precipitates suggest they did not form as a result of the weld solidification process. Rather, it appears these particles were transferred into the weld pool from the welding wire. To confirm this, Fig. 5 shows the microstructure of the Filler Metal 52 wire, where even larger TiN particles were observed. The larger size of the precipitates in the welding wire suggests that the nitrides partially dissolved once they were injected into the molten pool. Since the welds were made using the gas tungsten arc welding (GTAW) process with cold wire feed, it is possible for these particles to survive in the molten pool and then become entrapped in the microstructure during weld solidification.

The other precipitates, evident along the solidification subgrain boundaries in Fig. 3, are smaller (less than 1 µm in diameter), but are also rich in Ti and N. Analysis of these particles in the transmission electron microscope verified that they are TiN. Because these smaller precipitates are slightly elongated and perfectly aligned along the solidification subgrain boundaries, it is apparent that their formation is directly related with solidification segregation. It is hypothesized that these particles are the result of a eutectic reaction at the end of solidification, or may form in the solid state on cooling from the solidification range or during reheating in the multipass weld. Further study is necessary to clarify the nature of these particles.

Initially, these precipitates were thought to be MC carbides, Laves phase, or a mixture, which precipitate at the end of the solidification as a result of eutectic reactions (Ref. 9). Depending on the chemical composition of the alloy, MC carbide precipitation or MC carbide plus Laves phase may form in Ni-based weld metals, as proposed by DuPont and coworkers (Ref. 9). Figure 6 shows the schematic solidification path for an Nb-bearing Ni-based alloy, which leads to the formation of MC carbides (NbC in this case) and possibly Laves phases eutectic constituents during solidification. Compositionally, Laves phase can form from several elements in the basic form [(Ni, Fe, $Co)_2$(Nb, Ti, Mo)]. Energy-dispersive spectrometry analysis of the precipitates did not indicate any combination of Ni or Fe and Ti, which could be the most probable if Laves was present. Based on this cursory analysis, it appears that the predominant particle in the Filler Metal 52 weld microstructure is a Ti-rich nitride approximating TiN.

The detail of the grain boundary in Fig. 2 shows they have clearly migrated away from the solidification subgrain boundaries that are free of the TiN precipitates. Ductility-dip cracking is predominant along these "clean" migrated grain boundaries. The bottom photo in Fig. 2 is a higher magnification of the boxed area in the upper photo of Fig. 2, clearly illustrating the lack of precipitation or second phases along the migrated grain boundary, whereas the large TiN particles appear as single large cuboidal particles, as

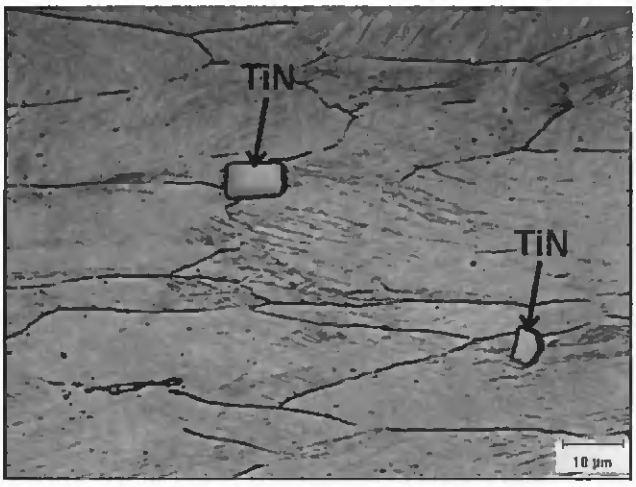

Fig. 5 — Second phases precipitated in the Filler Metal 52 weld metal.

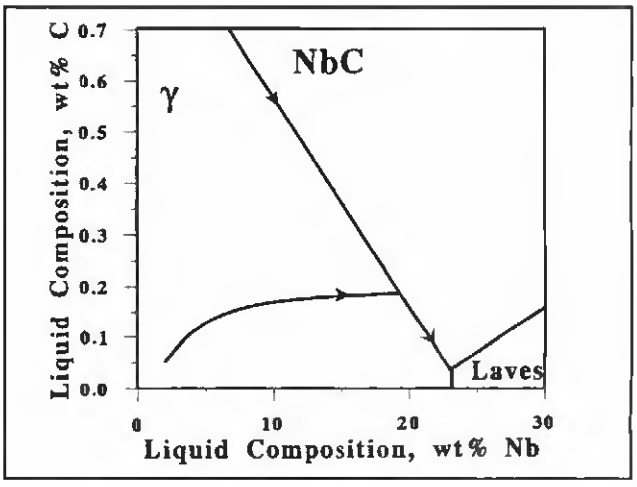

Fig. 6 — Schematic solidification path for a Nb-bearing superalloy leading to the formation of MC carbides and possibly Laves phases eutectic constituents (Ref. 5).

Table 2 — Filler Metal 82 Chemical Composition Comparison (wt-%)

Element	Ni-Cr-Fe-Nb Weld Deposit 12	Filler Metal 82 Heat YN6830	Differential (+ or −)
C	0.031	0.040	+0.009
Mn	0.20	2.86	+2.66
Fe	7.04	1.18	−5.86
S	0.007	0.01	+0.003
Si	0.16	0.12	−0.04
Cu	0.035	0.09	+0.055
Ni	73.85	72.75	−1.1
Al	0.12	N/A	—
Ti	0.26	0.37	+0.11
Cr	15.7	20.1	+4.4
Nb + Ta	1.58	2.3	+0.72
Mo	N/A	N/A	—
P	N/A	0.007	—
Pb	N/A	0.004	—
Co	N/A	0.05	—

shown in Fig. 3, and discrete small particles (see left portion of bottom photo in Fig. 2). Some other elongated phases appear continuous (see right portion of bottom photo in Fig. 2) along some of the solidification subgrain boundaries. The ductility-dip crack follows a migrated grain boundary path that both transects and directly follows a solidification subgrain boundary.

The grain boundary highlighted and detailed in Fig. 2 migrated from the relatively "clean" solidification subgrain boundary to its left. Since the precipitates were not prevalent along this particular solidification subgrain boundary, the impediment to boundary motion was low enough to allow the boundary to migrate. Migrated grain boundaries move away from the compositional portion of a solidification grain boundary in the solid state due to simple grain growth or a boundary straightening mechanism. Throughout the Filler Metal 52 microstructure, some regions reveal decreased microsegregation along the solidification subgrain boundaries and decreased second phases than do other regions. The "clean" grain boundaries or the grain boundaries absent of such constituents preferentially migrate and crack under sufficient levels of strain. Under low levels of applied strain, these "clean" boundaries are most likely the sites of DDC initiation with propagation possible along more tortuous boundary segments. The tortuous paths appear to assist in arresting DDC propagation, probably due in part to a mechanical "locking" effect.

Filler Metal 82

In comparison to Filler Metal 52, Filler Metal 82 migrated grain boundaries are always tortuous in nature, which contributes to an increased resistance to DDC (Ref. 4). Filler Metal 82 weld deposits contain large amounts of MC carbides (FCC crystal structure) of the type NbC and/or (Nb,Ti)C, which pin the grain boundaries. Thus, grain growth is inhibited resulting in increased grain boundary area and a subsequent increase in the strain necessary to cause cracking. The interdendritic position of these carbides suggest they are the result of a eutectic reaction occurring at the end of solidification, as schematically shown in Fig. 6. The solidification process in this alloy starts as L→γ with the interdendritic region or liquid becoming enriched in C and Nb, until the composition of this liquid achieves the twofold saturation between γ and NbC. At this point the solidification continues by the simultaneous formation of γ and NbC by a eutectic-type reaction as the remnant liquid follows the twofold saturation line shown in Fig. 6. If the solidification process ends along this twofold line, the only interdendritic-formed phase would be NbC. However, if solidification continues to the triple eutectic point (where γ, NbC, and Laves phases are in equilibrium) it will form Laves phase in addition to γ and NbC (Ref. 9). In the case of the Filler Metal 82 chemical composition (Table 2), the low Fe content limits the Laves formation and the results show that in this case the solidification ends along the twofold saturation line before the triple eutectic point is reached. As a result, only the NbC second phase is formed during solidification of Filler Metal 82.

In Filler Metal 82, eutectic carbides are evenly distributed throughout the microstructure, residing at solidification grain and subgrain boundaries. Figure 7 shows eutectic MC carbides consistently distributed throughout the Filler Metal 82 microstructure with several of the con-

stituents effectively pinning the grain boundary from further motion, thereby restricting grain growth. Additionally, Fig. 7 illustrates a number of smaller intergranular and intragranular carbides (see boxed area in lower photo of Fig. 7). These smaller precipitates were found to be associated with the interdendritic regions and gathered around the larger carbides. In contrast, the Filler Metal 52 weld deposit microstructure appears to be free of these groups of smaller precipitates when observed in the SEM.

EDS analysis of the large precipitates (Fig. 8) showed Nb and Ti peaks, characteristic of an Nb-Ti-rich MC carbide (Nb,Ti)C. The Ni and Cr peaks result from the electron beam interaction with the matrix due to the small size of the analyzed particle. The particles observed in the boxed area in the lower photo of Fig. 7 were too small to identify in the SEM, but have been identified independently as (Nb,Ti)C (Ref. 10).

Figure 9 reveals further definitive evidence of grain boundary pinning by the MC eutectic carbides. Again the large eutectic constituents are (Nb,Ti)C formed at the end of solidification. The smaller precipitates (in the boxed area and along the grain boundary) are most likely (Nb,Ti)C or some other type of MC-carbide particles.

Electron Backscattered Diffraction

Electron backscattered diffraction was used to determine the point-to-point local lattice orientation over the sample surface. Based on these data, information regarding the grain boundary misorientation, special orientation relationships such as coincident site lattice (CSL) grain boundaries, and accumulated plastic local strain was extracted from several STF samples in both the cracked and uncracked conditions.

Special Grain Boundaries. In general terms, the grain boundary character distribution (GBCD) determined using EBSD showed a small fraction of low-Σ CSL grain boundaries in the microstructure. The highest measured fraction of Σ_3–Σ_{29} was about 17%, which is not far away from the expected value for an as-welded austenitic material. However, this fraction is slightly higher than the 9.1% reported for as-cast, pure nickel (Ref. 11).

The GBCDs measured on the STF samples of Filler Metal 52 and Filler Metal 82 (Heat YN6830) are summarized in Table 3. The data in this table should be analyzed carefully because important differences exist among different regions of the samples. Measurements 2, 5, and 6 were conducted on cracked samples but in regions where cracks were not present. All the other measurements were taken in regions where many cracks were present.

When the measurements were performed in uncracked regions (measurements 2, 5, and 6 in Table 3) or over larger regions where the cracked area represented a lower fraction (measurement 4), the low-Σ CSL grain boundary fraction was lower, as can be seen when measurement 3 is compared with measurements 5 and 6, or when comparing measurements 3 and 4 (larger region with lower cracked area). The only exception was measurement 2, where the uncracked region of Filler Metal 52 had a relatively high (12.2%) fraction of low-Σ CSL grain boundaries. This result was probably due to the poor statistics of measurement 2, resulting from the large grain size. However, this sample was tested at high temperature (1160°C) where the higher fraction of low-Σ CSL grain boundaries may be explained by the observed dynamic recrystallization.

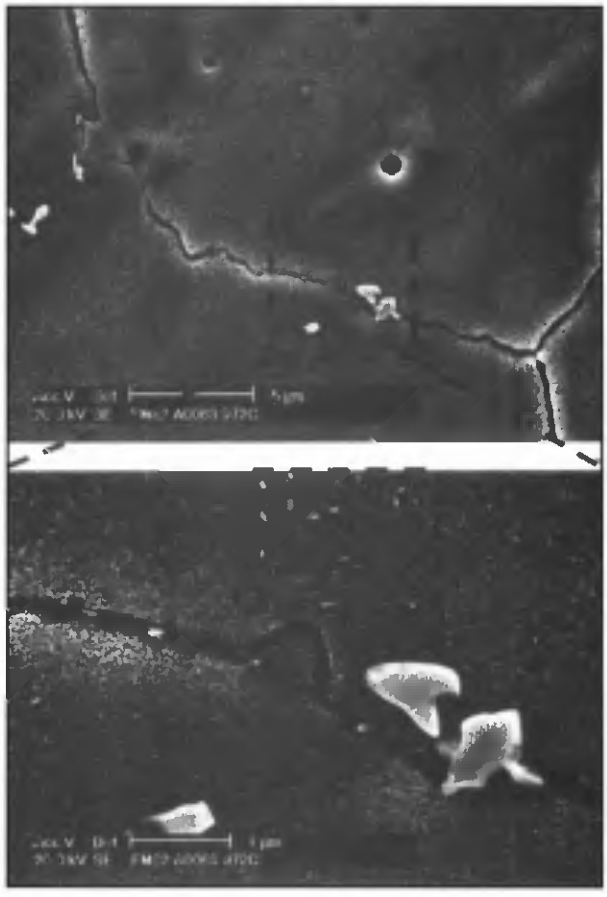

Fig. 7 — Tortuous boundary in Filler Metal 82 resulting from "pinning" by eutectic particles. (Boxed area in lower photo shows small particles prevalent throughout the Filler Metal 82 weld-metal matrix.)

The GBCD data show that the special grain boundaries are mainly associated with the regions that have cracks and not with the uncracked regions. This result appears to be contradictory with the accepted higher cracking resistance of these special grain boundaries. However, the special grain boundaries observed around the cracks were formed during the dynamic recrystallization process suffered by these highly deformed regions around the intergranular cracks. It should be noted that the fraction of special grain boundaries in the microstructure was too low to significantly influence the crack nucleation.

The misorientation between the grains where intergranular cracking occurs was measured in the samples subjected to EBSD analysis. The results of these measurements are presented in Table 4. The angle between these grains varied between 9 and 60 deg, with the average approximately 40 deg. This value is close to the maximum misorientation frequency, expected to be about 45 deg, for a theoretical random set of misorientations. Therefore, the cracked grain boundaries were random grain boundaries. In addition, an EBSD orientation map reconstruction, by extrapolation of the grain orientations around the cracks, verified that the cracked grain boundaries were not low-CSL grain boundaries, as expected, due to the reported high cracking resistance of these grain boundaries.

Strain Distribution

The EBSD technique also allows the local strain distribution in the microstructure to be estimated, allowing strain maps to be plotted. The strain maps from STF specimens revealed strain concentration at or very near the grain boundaries, especially at the triple-point junctions. When cracked regions were mapped, as shown in Fig. 10, strain concentration around the cracks was evident. Figure 10 presents the strain map in an STF specimen of Filler Metal 52 heated to 986°C and strained 2.6%. In this map, the thin lines represent the high angle grain boundaries and the black regions are the open cracks from which EBSD information is not obtained. The color pattern represents the strain distribution, with blue representing the lowest and red the highest strains in this map. In all the strain maps developed

Table 3 — Grain Boundary Character Distribution of STF Samples

Measurement	1	2	3	4	5	6	7	8
Alloy	FM-52	FM-52	FM-82	FM-82	FM-82	FM-82	FM-82	FM-82
Temperature (°C)	986	1160	972	972	984	984	1147	1147
Strain (%)	2.6	2.9	7.5	7.5	8.1	8.1	11.3	11.3
Area (mm x mm)	0.4 x 0.3	0.4 x 0.3	0.4 x 0.3	2.0 x 1.8	0.7 x 0.5	0.4 x 0.3	0.4 x 0.3	0.4 x 0.3
Cracks	Yes	No	Yes	Yes	No	No	Yes	Yes
	CSL Σ_{n3} fraction of the high angle grain boundaries (angle > 15 deg) [%]							
Σ3	3.9	2.1	5.9	2.9	0.3	0.3	10.3	8.7
Σ5	2.2	—	—	1.6	0.1	1.3	0.3	0.4
Σ7	—	—	0.5	0.9	—	0.7	1.2	—
Σ9	2.5	—	0.2	0.6	—	—	0.4	0.3
Σ11	0.3	0.1	0.1	0.5	—	—	—	-
Σ13	0.1	—	1.1	0.4	3.4	—	1.1	—
Σ15	0.3	—	1.6	0.2	—	0.5	0.1	1.6
Σ17	2.0	—	—	0.4	—	—	0.2	0.4
Σ19	0.1	3.4	0.6	0.1	—	—	0.7	0.9
Σ21	0.1	6.5	0.3	0.2	—	—	0.4	0.7
Σ23	0.1	—	0.2	0.3	—	—	-	—
Σ25	—	—	0.8	0.2	—	—	0.1	0.4
Σ27	0.1	—	0.2	0.7	—	0.1	0.1	0.4
Σ29	—	—	0.1	0.3	2.8	4.4	2.3	2.5
Total (%)	11.6	12.2	11.5	9.2	6.7	7.3	17.0	16.4

Table 4 — Grain Boundary Misorientation in STF Samples

Measurement	1	3	4	7	8
Alloy	FM-52	FM-82	FM-82	FM-82	FM-82
Heat	NX9277	YN6830	YN6830	YN6830	YN6830
Temperature (°C)	986	972	972	1147	1147
Strain(%)	2.6	7.5	7.5	11.3	11.3
Area (mm x mm)	0.4 x 0.3	0.4 x 0.3	0.2 x 1.8	0.4 x 0.3	0.4 x 0.3
	Misorientation between grains where cracking occurred (degrees)				
Minimum	9	20	21	19	11
Maximum	54	60	52	57	59
Average	40 ± 10	40 ± 5	34 ± 3	40 ± 5	39 ± 4

from STF specimens of Filler Metals 82 and 52, the strain was found to be concentrated at the grain boundaries with essentially no strain in the grain interiors. The highest strains were associated with the crack tips, where high stress concentrations would be expected.

Discussion

Based on the results presented here and those from Parts I and II of this investigation, it is clear that DDC is a complex phenomenon that is influenced by multiple factors, to be reviewed and discussed in the following sections. Reference to Parts I and II of this investigation are suggested in order to understand the entire context of this discussion.

Alloy Element Effects

Based on the results of STF tests presented in Part I of this investigation, significant differences in DDC susceptibility were observed when comparing Filler Metals 52 and 82. Data in the literature support the observed differences based on the composition of the weld metal. A number of Ni-based alloy welds were tested by Heuschkel (Ref. 12) to determine their elevated-temperature ductility response. In that study, Ni-Cr-Fe-Nb weld deposits achieved the best ductility, with a minimum elongation of 34% observed. Conversely, Ni-Cr-Fe-Ti and Ni-Cu-Ti type weld deposits exhibited the lowest ductility, with a minimum elongation of 10% reported. The 649°–1093°C low-ductility temperature range reported for the Ni-Cr-Fe-Nb weld deposits is similar to the STF results for Filler Metal 82 (Ref. 4), which contains Nb and forms a NbC eutectic constituent. Interestingly, the Ni-Cr-Fe-Ti weld metal contained only 0.47% Nb while the Ni-Cu-Ti weld deposits contained no Nb additions whatsoever. Table 2 compares the composition of the Ni-Cr-Fe-Nb weld deposits from Heuschkel (Ref. 12) with that of Filler Metal 82 (Heat YN6830).

Overall, the compositions of the two filler metals (Table 2) are strikingly similar. Note especially the Nb, Cr, and C contents. From his studies of a number of differently alloyed Ni-Cr-Fe weld deposits, Heuschkel (Ref. 12) reported the best results for those weld deposits containing Nb additions and made with argon shielding gas. Additionally, Sadowski (Ref. 13) summarized the effects of Nb on weld-metal hot cracking susceptibility of 25%Cr-20%Ni based on reports by several authors and reported Nb content to be deleterious up to 0.25% while beneficial at 1.38–2.90%. This is precisely the Nb range for both filler metals in Table 2. Furthermore, based on hot ductility testing of 25%Cr-20%Ni and 18%Cr-8%Ni, Haddrill and Baker (Ref. 14) reported that Nb-containing weld deposits increased the observed ductility minimum significantly compared to weld deposits free of Nb additions.

Carbon content has been reported by a number of researchers to have a significant effect on DDC susceptibility (Refs. 2, 14–16). Haddrill and Baker (Ref. 14) observed less cracking along migrated grain boundaries as carbon content was increased from 0.06 to 0.125 wt-% in reheated regions of 25%Cr-20%Ni austenitic weld metal. They suggested that the reduction in cracking susceptibility with the increased interstitial element content could be related with the morphology and distribution of the intergranular carbides and with the segregation of solute elements to the dislocations. In support of this, Matsuda et al. (Ref. 15) and Arata et al. (Ref. 16) reported a much narrower DTR and an increased minimum strain

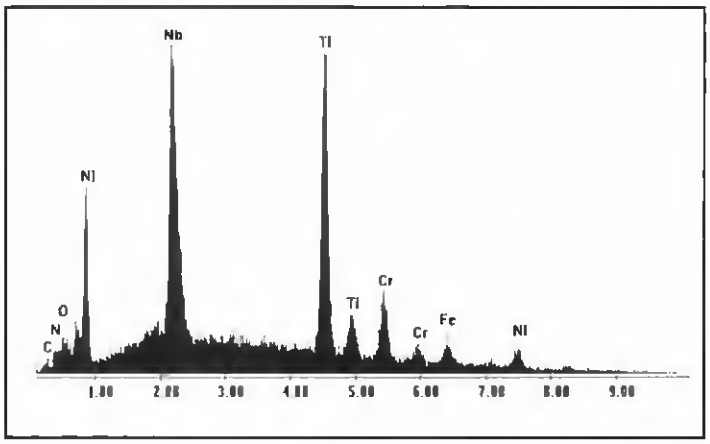

Fig. 8 — EDS analysis of large eutectic constituents along the migrated grain boundaries in Filler Metal 82.

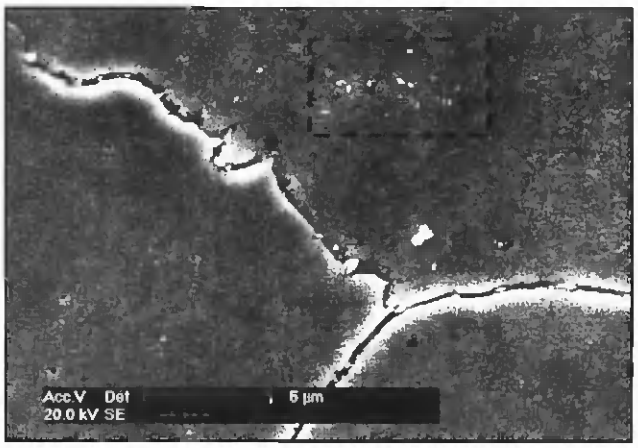

Fig. 9 — Triple-point migrated grain boundary intersection with eutectic grain boundary "pinning" in Filler Metal 82 tested at 1147°C.

(E_{min}) to cause cracking in fully austenitic 310S when carbon contents were increased, with no DTR phenomena observed whatsoever when carbon contents ranged between 0.43 and 0.53%. This improvement in ductility was attributed to an increase in the formation of eutectic M_7C_3 carbides that restrict grain growth and grain boundary mobility (Refs. 12, 17).

Nickel-based alloys containing Nb can form both MC carbides and Laves phase eutectic constituents during solidification (Ref. 9). However, thermodynamic calculations showed that for the chemical compositions of Filler Metals 52 and 82, the formation of eutectic Laves phase is not expected. In the case of Filler Metal 52, the calculations showed that the slightly higher content of Ti, along with the N content, promotes TiN (FCC structure) precipitation in the liquid and its continuous precipitation along the entire solidification range. The chemical composition of this precipitate gradually changes from TiN at temperatures well above the alloy liquidus to NbC (FCC structure) at the end of the solidification. Thermo-Calc™ estimates of the simulated solidification paths revealed the mass fraction of TiN+(Nb,Ti)C at the end of the solidification to be approximately 0.25% for Filler Metal 82 and 0.1% for Filler Metal 52 (Ref. 10). The actual fraction of eutectic constituents was not measured, but a qualitative analysis shows there is a large difference in the fraction of these interdendritic precipitates, being much smaller and less uniformly distributed in Filler Metal 52.

Based on observations made during this investigation, it is postulated that the difference in STF DDC susceptibility between Filler Metal 52 and Filler Metal 82 is explained, in part, by the different contents of Nb and C. These contents are higher for Filler Metal 82, and therefore its ability to form MC-type carbides is increased. The interdendritic constituents inhibit grain boundary motion in the solid state resulting in smaller grains and increasingly tortuous grain boundary paths that are resistant to cracking. These constituents along the boundary also inhibit grain boundary sliding, which has been reported to be most prevalent along "clean" grain boundaries (Refs. 18–22).

Hydrogen Effects

Hydrogen was shown to have a pronounced negative effect on the STF behavior of Filler Metal 82, as discussed in Part I and II of this investigation (Refs. 4, 5). Hydrogen cracking is typically not a concern in fully austenitic structures based on the high solubility of hydrogen and its low diffusivity in the austenitic (FCC) matrix. Regardless, atomic hydrogen is an extremely mobile interstitial species and hydrogen cracking may occur in austenitic materials if sufficient hydrogen is present (Ref. 23). Part II of this investigation (Ref. 5) contained a discussion of the two different H-embrittlement mechanisms, hydrogen-enhanced local plasticity (Ref. 24) and hydrogen-induced decohesion (Ref. 25), and that may be acting in the DDC temperature range of these filler metal deposits. The high incidence of triple-point cracking along with the planar slip evident in the fractography of the STF samples with intentional hydrogen additions suggests that both hydrogen embrittlement mechanisms may be operative during DDC of Ni-based alloys. The level of hydrogen necessary to reduce ductility in addition to the effect of grain boundary structure and precipitation on hydrogen mobility is the subject of continuing research.

Eutectic Constituent Effects

In addition to the large cuboidal TiN transferred from the weld wire (Figs. 3 and 5), Filler Metal 52 formed small nitrides during solidification. Based on thermodynamic calculations, the eutectic phase formed at the end of solidification was the isomorph MC carbide, having the same crystal structure as TiN with very similar lattice parameters. The gradual change of the precipitated phases from TiN to MC has been previously reported during the solidification of N-bearing Ni-based superalloys (Ref. 26). The weight fraction of the interdendritic phases in Filler Metal 52 was very low (about 0.1% according to thermodynamic calculations) and its distribution within the weld metal microstructure was very inconsistent (Figs. 1 and 2) resulting in relatively large areas across the weld metal microstructure that were absent of boundary "locking" and/or "pinning" constituents. As a result, Filler Metal 52 exhibited many long, straight, "clean" migrated grain boundaries that crack under low levels of strain (<2%).

In contrast, Filler Metal 82 forms abundant MC-carbide eutectic constituents of the type (Nb,Ti)C. The calculated weight fraction of this carbide for Filler Metal 82 was approximately 0.25% (Ref. 10). The carbides were distributed relatively consistently throughout the weld metal microstructure (see Figs. 7 and 9) further inhibiting boundary motion and grain growth, and thus decreasing cracking susceptibility.

It is apparent that boundary tortuosity plays an important role in the DDC susceptibility of the weld metal, especially at low levels of applied strain. In these filler metals, tortuosity is associated with the (Nb,Ti)C eutectic carbide when higher levels of carbon and Nb are present in the filler material. Increased eutectic constituents in the microstructure reduce grain growth, increase grain boundary tortuosity, and significantly suppress grain boundary sliding resulting in increased resistance to DDC initiation and propagation. Based on the STF results for these

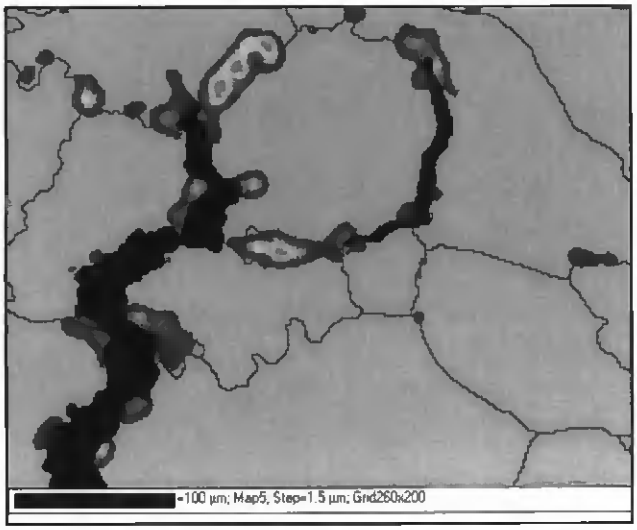

Fig. 10 — Strain distribution map in the STF specimen of Filler Metal 52 heated to 986°C and strained 2.6%. The thin lines represent the high angle grain boundaries. The black regions are the open cracks. The colored contouring shows the strain distribution with blue representing the lowest and red the highest strains.

filler metals, a strong contributing factor to the higher resistance of Filler Metal 82 to DDC is the preponderance of tortuous migrated grain boundaries. These tortuous boundaries provide a mechanical locking effect as the adjacent crystals attempt to slide past each other with applied strain at elevated temperature.

The specific effect of different interdendritic particles, i.e., nitrides, carbides, or other particles, on the variation in cracking behavior between Filler Metals 52 and 82 is not clear. It is possible that certain particles are more effective in reducing DDC relative to others based on their size, distribution, or morphology. This effect is also the subject of ongoing research.

Segregation Effects

In Part I of this investigation, the detrimental effect of sulfur on DDC was clearly shown. Although detailed grain boundary analysis was not performed, it is anticipated that the segregation of sulfur to the migrated grain boundaries was responsible for this degradation. In addition, as described previously, the accumulation of hydrogen at grain boundaries also appears to be detrimental.

Migrated grain boundaries move more easily through the weld metal microstructure when fewer eutectic constituents are present to "lock" and/or "pin" grain boundary motion. During multipass welding, multiple thermal cycles promote additional boundary migration and segregation. During migration, impurity and interstitial elements can be swept into the boundary as they have high diffusivities and high affinities for grain boundaries. As the impurity and interstitial content in the boundary approaches a critical level, a "drag effect" is imposed upon the boundary. The boundary is no longer highly mobile but is now highly enriched in impurity and interstitial element content. This enrichment may have negative implications as some impurity and interstitial elements are detrimental to ductility. Thus, in the event that impurity and interstitial segregation play roles in the DDC mechanism, less grain boundary area brought about by increased grain size will lead to higher impurity and interstitial concentrations at the grain boundaries, possibly lowering cohesion between grains. Such an increase in segregation could further weaken the grain boundaries, encouraging grain boundary sliding under low orders of strain, subsequently resulting in intergranular cracking.

Effect of Triple-Point Junctions

The presence of triple-point grain boundary intersections in polycrystalline materials has been shown to influence several material properties, including ductility, grain boundary migration, sliding, and recrystallization (Refs. 11, 27). Watanabe (Ref. 11) used a computer simulation of intrinsic stress distributions at triple-point grain boundary intersections to show that uncompensated stresses exist at these intersections, supporting the hypothesis that triple-point grain boundary intersections are highly stressed regions conducive to crack initiation.

Masubuchi and Martin (Ref. 18) and Haddrill and Baker (Refs. 14, 22) describe cracking along triple-point grain boundary intersections and attribute the cracks to a combination of increased stress concentration at the intersection and grain boundary sliding. Masubuchi and Martin (Ref. 18) stated that sliding along grain boundaries might take place at a low stress since the inherent grain boundary flow stress is very low. Thus, the high stress concentration at the intersection initiates intergranular fracture with propagation of the fracture a function of sliding along the low flow stress grain boundary. Ductility-dip cracking appears to either initiate or terminate at these intersections. The strain maps obtained by EBSD, such as the one presented in Fig. 10, clearly reveal strain concentration at triple points. It is possible that cracking initiates at these triple-point grain boundary intersections, as these are sites of high stress concentration, thereby lowering the "global" stress necessary to initiate cracking.

Dynamic Recrystallization

A combination of accumulated deformation and thermal energy promotes recrystallization. High local strains at the crack tip lower the amount of thermal energy necessary to induce recrystallization. The strain maps obtained from the cracked samples reveal recrystallization occurring at the strain-concentrated regions of the microstructure, either in front of the cracks or at the triple-point junctions along the crack path. Figure 10 shows two regions of strain concentration where recrystallization has initiated, one of them in front of the smaller crack and the other where the larger crack changed its propagation direction due to a triple point. Additionally, strain concentrates along grain boundaries that have not separated. As temperature increases, recrystallization occurs more easily at these strained grain boundaries. Based on observations during this investigation, it is postulated that the combination of applied strain, stress concentration at the grain boundary, high local strains at the crack tip, and applied thermal energy increases the likelihood of dynamic recrystallization. Therefore, it is possible that the appearance of dynamic recrystallization within the microstructure signals the onset of ductility recovery in the high-temperature region (1050°–1200°C) of the overall DTR.

Boundary Orientation Relative to the Applied Strain

It is apparent that grain boundary orientation to the applied strain is a factor in DDC formation. Previous studies by Bowers (Ref. 28) and Kikel and Parker (Ref. 29) using the double-spot Varestraint test showed that orientation relative to the applied strain has a significant effect on DDC susceptibility. In this investigation, STF samples were tested in both the as-welded (multipass weld) and spot-welded condition. The as-welded condition results in a more random grain boundary pattern resulting from epitaxial nucleation and columnar grain growth in the multipass weld. When a spot weld is made within the weld metal in the STF sample, a radial grain boundary pattern is created with boundaries ranging from 0 to 90 deg relative to the applied strain. For Filler Metal 52, the as-welded STF behavior showed a threshold strain of 2.5%, but when spot-welded samples were tested the

threshold strain for cracking dropped to 1%. There are other metallurgical influences that complicate this simple argument, such as the effect of multiple reheating in the multipass weld on the nature of the boundary. However, based on the observation that most DDC is observed in the spot welds in the angular range of 45–90 deg to the applied strain, it can be concluded that the macroscopic boundary orientation in the weld metal relative to the applied strain is a contributing factor to DDC.

Fracture Morphology

Part II of this investigation described the fracture behavior associated with DDC in STF samples of Filler Metals 52 and 82 throughout the entire 625°–1200°C DDC temperature range (Ref. 5). Ductility recovery at both extremes of the DTR is marked by ductile intergranular fracture. The ductility recovery at elevated temperature coincides with the onset of local recrystallization at the grain boundaries. In the intermediate temperature regime of the DTR, the intergranular fracture acquires a wavy pattern with crystallographic steps superimposed. These steps are clearly evidence of crystalline slip, which is thought to be related with the hydrogen-induced plasticity. The presence of precipitates was evident on the fracture surfaces. However, the exact relationship between fracture behavior and grain boundary precipitation is still not clear and is the subject of an ongoing investigation.

Grain Boundary Character Distribution

It is well known that low CSL grain boundaries (Σ_3–Σ_{29}) exhibit special properties that are associated with the relatively good atomic scale matching and consequently low energy of these grain boundaries. Among these special properties are high resistance to 1) crack propagation, 2) localized corrosion, 3) sliding and cavitation at high temperatures, and 4) lower solute segregation (Refs. 11, 27). Ductility-dip cracking is a high-temperature phenomenon and, although the difference in properties between the low-Σ CSL and the random grain boundaries decreases when temperature increases (Ref. 30), the effect of CSL grain boundaries on the DDC phenomenon was of interest.

Although a high fraction of "special grain boundaries" was not observed in either of the filler metals (Table 2), most of the boundaries identified were low Σ-CSL grain boundaries (Σ_3, Σ_5, Σ_9, and Σ_{29}), to which special properties have been reported (Refs. 11, 27). These boundary types have low activity levels in relation to grain boundary migration, sliding, vacancy generation, diffusion, and absorption while high-angle "random" grain boundaries have high activity levels in relation to these boundary characteristics (Ref. 11). Cracking did not occur along any of the "special" grain boundaries with some boundaries appearing to arrest crack propagation.

In support of this observation, Watanabe (Ref. 11) reported that "special" grain boundaries are strong obstacles to crack propagation such that intergranular fracture will arrest at these boundary types. In almost all cases, DDC was observed along "random" high-angle grain boundaries. Based on the high activity levels associated with these boundaries, fracture along these boundary types is not surprising.

Further supporting the fracture resistance of low-Σ CSL boundaries and low-angle boundaries, Palumbo and Aust (Ref. 27) reported that these boundary types would not fracture even when lying at optimal angles (45–90 deg) for operation of a grain boundary sliding assisted fracture mechanism. These angles are precisely the angular orientation range to the applied load found to be typical for DDC along random high-angle migrated grain boundaries in Filler Metals 52 and 82, further supporting fracture propensity along high-energy, high-angle migrated grain boundaries.

Grain boundary cracking resistance decreases as the boundary becomes more "random" (i.e., deviating further away from low energy configurations). At the same time, the potential for segregation of solute and impurities to this grain boundary is also enhanced (Ref. 11). The higher energy level of the boundary also improves its mobility, generating synergy between the potential for segregation of the boundary and the "sweeping" effect of impurities while it moves. This behavior lends support to increasing eutectic constituent content and decreasing impurity content in the weld-metal microstructure. Increased eutectic constituent content will inhibit boundary migration and the consequent sweeping of impurities, further minimizing the probability of grain boundary sliding and/or cracking.

In the STF samples, most of the special grain boundaries present in the microstructure were a result of the thermomechanical work, which occurred during the test itself. Many of these special grain boundaries appeared to originate during the recrystallization process in the highly strained material around the cracks. Based on this observation, low-Σ CSL boundaries have little effect on crack initiation, but may play an important role in the crack arrest process.

Insight into the DDC Mechanism

While the mechanism for DDC is still not fully understood, the STF test has confirmed many previous theories about DDC and has proven itself as a valuable method to test different conditions and produce a variety of cracked samples for evaluation. Results from this investigation confirm that DDC occurs preferentially along weld-metal migrated grain boundaries. An overwhelming majority of DDC was observed in the spot weld with cracks occurring outside the spot weld in multipass weld metal only at relatively high strains (>8%). Typically, cracks occurred on migrated grain boundaries oriented approximately 45–90 deg to the applied strain. These results agree with previous reports that grain boundary orientation relative to the direction of the applied strain is a contributing factor to formation of DDC (Refs. 15, 19, 29, 31).

The effect of intergranular precipitation on grain boundary sliding remains controversial. Mathew et al. (Ref. 21) and Dix and Savage (Ref. 32) postulated that as grain boundary precipitates form, grain boundary sliding is restricted enabling significant matrix deformation and higher ductility. Conversely, Zhang et al. (Ref. 33), Mintz et al. (Ref. 17), and Arata et al. (Ref. 16) concluded that increased intergranular precipitation lowers grain boundary ductility.

Materials containing precipitates, eutectic constituents, and/or second phases tend to restrict grain boundary motion and thereby reduce the amount and length of cracking. Furthermore, formation of eutectic constituents at the end of solidification results in tortuous grain boundary paths that are increasingly resistant to both DDC initiation and propagation when compared to straight grain boundary paths free of precipitates. Tortuous grain boundary paths result in increased grain boundary area vs. straight grain boundaries, over a given length. Grain boundary sliding is impeded by tortuous boundaries and orientation to the applied strain is increasingly random vs. a straight grain boundary oriented favorably for DDC formation.

Previous research supports the concept of Nb and C additions to the weld metal to decrease cracking susceptibility (Refs. 2, 12–16). Increased C contents in Filler Metal 82 may result in increased MC-carbide (NbC) formation along grain boundaries that further restrict grain growth and grain boundary migration ultimately resulting in increased grain boundary area to withstand higher applied strains. This investigation supports the hypothesis that grain boundary precipitates act as locking points along the boundary, thereby restricting grain boundary sliding and enabling significant matrix deformation and higher ductility (Refs. 21, 32). Furthermore, restricted boundary motion resulting from pinning by eutectic constituents

in the microstructure results in reduced "sweeping" of impurities and undesirable solute elements into the boundary, further enhancing resistance to DDC.

Zhang et al. (Refs. 33, 34) revealed that fully austenitic stainless steel weld metals precipitated $M_{23}C_6$ carbides along migrated grain boundaries below 1200°C, while also observing a high density of intergranular precipitation in Fe-36%Ni weld metals. Generally, it was observed that the prevalence of precipitates increased at locations where migrated grain boundaries intersect solidification subgrain boundaries. Subsequently, it was postulated that since the solute concentration at the solidification subgrain boundary is high, migrated grain boundary precipitation should easily occur at this intersection. It was also determined that a certain region of the migrated grain boundary near the intersection could be enriched by solute elements due to rapid diffusion at the grain boundary intersection. These observations further support the hypothesis that as grain boundary precipitates form, grain boundary sliding is restricted, enabling significant matrix deformation and higher ductility.

Controlling impurity contents (S, P, etc.) may also assist in controlling formation of DDC, especially during multipass welding operations. Based on the increase in DDC susceptibility observed during STF testing of Filler Metal 82 with additions of sulfur to the spot weld, it is anticipated that minimizing S, P, and other impurity contents in Filler Metals 82 and 52 will increase the resistance to DDC. Cordea et al. (Ref. 31) concluded that after extensive grain growth, impurities became sufficiently concentrated on the grain boundaries to weaken them, resulting in crack initiation. As microsegregation of S, P, and other impurity elements easily occurs to solidification subgrain boundaries during solidification and diffusion along these boundaries is enhanced in comparison to the matrix, it is anticipated that the intersection of a migrated grain boundary with a solidification subgrain boundary will result in enrichment of impurity elements along the migrated grain boundary. This in turn will promote decohesion and facilitate grain boundary sliding along the boundary/matrix interface. Eliminating or minimizing impurity elements in the filler materials may assist in increasing the amount of strain necessary to initiate grain boundary sliding.

The potent effect of hydrogen on DDC susceptibility was initially quite surprising based on the perceived resistance of austenitic microstructures to hydrogen-induced cracking. Although the exact levels of diffusible hydrogen were not determined, it is estimated based on data gathered from multipass welds using 95Ar-5H_2 shielding gas (Ref. 35) that the levels were on the order of 15–20 ppm. It is proposed that this hydrogen is trapped within the microstructure at trap sites such as the carbide/matrix interface and then released upon heating above 625°C. Since many of the carbides are present along the grain boundaries and stress is concentrated at these boundaries, the hydrogen accumulates in the boundary and reduces its cohesive strength and activates the localized plasticity around the grain boundaries. It is conceivable that the DDC mechanism is simply a manifestation of hydrogen-assisted cracking at elevated temperature.

Welding speed was very low for the butter passes (2 in./min) and relatively low for the fill passes (5 in./min) during STF sample preparation. Yeniscavich (Ref. 36) used the hot ductility test to study the effects of welding speed on ductility response in Ni-Cr-Fe alloy wrought materials and weld metals. The results show significant differences in the ductility responses of wrought and welded specimens, indicating that microstructure is a significant parameter affecting hot ductility. Although somewhat mixed, data from a number of heats revealed that the ductility response is a function of welding speed with ductility typically increasing as welding speed increased from 1 to 10 in./min. Higher welding speeds produced finer grain sizes in both the fusion zone and heat-affected zone resulting in greater fissure resistance. Faster welding speeds not only produced a fissure-resistant structure, but also reduced the volume of material susceptible to fissuring. Furthermore, Yeniscavich postulated that segregation decreased as the welding speed increased, decreasing the likelihood of a low ductility response.

This investigation into DDC of nickel-based alloy filler materials has identified a number of factors that contribute to DDC formation. The DDC mechanism is most likely a complex interplay amongst these contributing factors rather than a result of any single factor. The research performed in this investigation has provided increased insight into a number of variables that can be manipulated to assist in decreasing or controlling DDC formation.

Control of the DDC mechanism may be effectively described by the following: Materials containing a consistent distribution of grain boundary precipitates and/or eutectic constituents effectively "lock" and/or "pin" grain boundary motion, inhibiting grain growth. Grain boundary tortuosity is therefore increased resulting in increased boundary area per unit length (vs. a straight grain boundary) to resist applied strains while also subjecting less of the grain boundary to orientations favorable to boundary separation. Precipitation, eutectic constituent formation, and subsequent grain boundary tortuosity effectively disrupt grain boundary sliding as cohesion between grains is enhanced. Impurity and solute segregation is effectively reduced as the "locked" and/or "pinned" boundary maintains a low-angle orientation that is more resistant to solute and impurity segregation as grain boundary "sweeping" of these detrimental elements is effectively controlled. Furthermore, controlling or eliminating impurity contents and utilizing high welding speeds control intergranular segregation during multipass welding operations, further increasing resistance to grain boundary decohesion and sliding. Controlling or eliminating a single factor contributing to the DDC mechanism will assist in preventing formation of DDC, but comprehensive control of all of the contributing factors will most likely result in the most optimal ductility response in nickel-based alloy filler materials.

Conclusions

1. Ductility-dip cracking occurred along random high-angle grain boundaries, generally referred to as migrated grain boundaries in austenitic weld metal.

2. A low fraction of interdendritic constituents (TiN) and eutectic MC-carbides were inconsistently distributed throughout the microstructure of Filler Metal 52 resulting in long, straight migrated grain boundaries. These boundaries have low resistance to grain boundary sliding and thus exhibited increased susceptibility to DDC.

3. A higher fraction of eutectic constituents, particularly (Nb,Ti)C, were distributed throughout the microstructure of Filler Metal 82 resulting in formation of tortuous grain boundary paths that are more resistant to DDC. The increased resistance to DDC was a function of the eutectic constituents "pinning" grain boundary motion effectively minimizing grain growth and grain boundary sliding.

4. Sulfur and hydrogen additions were found to increase susceptibility to DDC in Filler Metal 82.

5. Triple-point grain boundary intersections act as high stress concentration regions conducive to crack initiation. The addition of hydrogen greatly increased the incidence of cracking at triple points.

6. Straight migrated grain boundaries crack under low levels of strain (<2%). Higher levels of strain (>2%) are necessary to initiate cracking along tortuous migrated grain boundaries.

7. Recrystallization was observed in the upper temperature range (1050°–1200°C) of the DTR and coincided with ductility recovery.

8. Grain boundary orientation to the applied strain is a contributing factor to

DDC formation. Boundaries oriented at 45–90 deg to the applied strain were found to be most susceptible to DDC.

9. Using the EBSD technique, it was shown that high strain concentrations are present along the migrated grain boundaries upon application of only small strains in the STF test.

Acknowledgments

The authors would like to thank Nathan Nissley, Dan Ryan, and Shu Shi, members of the Welding and Joining Metallurgy Group at The Ohio State University, for their valuable assistance during this investigation. We are grateful for the technical input and guidance of Jeff Kikel and financial support by BWX Technologies, Inc.

References

1. Nissley, N. E. 2002. *Development of the Strain-to-Fracture Test to Study Ductility-Dip Cracking in Austenitic Alloys.* MS thesis. Columbus, Ohio: The Ohio State University.

2. Hemsworth, B., Boniszewski, T., and Eaton, N. F. 1969. Classification and definition of high-temperature welding cracks in alloys. *Metal Construction and British Welding Journal*, pp. 5–16.

3. Honeycombe, J., and Gooch, T. G. 1970. Microcracking in fully austenitic stainless steel weld metal. *Metal Construction and British Welding Journal* (9): 375–380.

4. Collins, M. G., and Lippold, J. C. 2002. An investigation of ductility-dip cracking in nickel-based filler materials — Part I. *Welding Journal* 82(10): 288-s to 295-s..

5. Collins, M. G., Ramirez, A. J., and Lippold, J. C. An investigation of ductility-dip cracking in nickel-based filler materials — Part II. *Welding Journal* 82(12): 348-s to 354-s.

6. Schwartz, A. J., Kumar, M., and Adams, B. (eds.). 2000. *Electron Backscattered Diffraction in Materials Science.* Kluwer Academic/Plenum Publishers, p. 339.

7. Gourgues, A. F. 2002. Electron backscattered diffraction and cracking, *Materials Science and Technology* 18(2): 119–133.

8. Lehockey, E. M., Lin, Y. P., and Lepik, O. E. 2000. Mapping residual plastic strain in materials using electron backscatter diffraction. *Electron Backscattered Diffraction in Materials Science*, A. J. Schwartz et al. (eds.). Kluwer Academic/Plenum Publishers, pp. 247–264.

9. DuPont, J. N., Robino, C. V., and Marder, A. R. 1998. Solidification and weldability of Nb-bearing superalloys, *Welding Journal* 77(10): 417-s to 431-s.

10. Ramirez, A. J. 2002. Unpublished research performed at The Ohio State University.

11. Watanabe, T. 1988. The potential for grain boundary design in materials development. *Materials Forum* (11): 284–300.

12. Heuschkel, J. 1960. Weld metals in nickel-base alloys. *Welding Journal* 39(6): 236-s to 246-s.

13. Sadowski, E. P. 1974. Modification of cast 25Cr-20Ni for improved crack resistance. *Welding Journal* 53(2): 49-s to 58-s.

14. Hadrill, D. M., and Baker, R. G. 1965. Microcracking in austenitic weld metal. *British Welding Journal* 12(8) 411–419

15. Matsuda, F. 1990. Hot crack susceptibility of weld metal. *Proceedings of the 1st U.S.-Japan Symposium on Advances in Welding Metallurgy*. Miami, Fla.: American Welding Society, pp. 19–36.

16. Arata, Y., Matsuda, F., and Katayama, S. 1977. Solidification crack susceptibility in weld metals of fully austenitic stainless steels (Report II) — Effect of ferrite, P, S, C, Si and Mn on ductility properties of solidification brittleness. *Transactions of JWRI* 6(1): 105–117.

17. Mintz, B., Abu-Shosha, R., and Shaker, M. 1993, Influence of deformation induced ferrite, grain boundary sliding and dynamic recrystallization on hot ductility of 0.1–0.75%C steels. *Materials Science and Technology* 9(10): 907–914.

18. Masubuchi, K., and Martin, D. C. 1962. Mechanisms of cracking in HY-80 steel weldments. *Welding Journal* 41(8): 375-s to 384-s.

19. Rhines, F. N., and Wray, P. J. 1961. Investigation of the intermediate temperature ductility minimum in metals. *Transactions of the ASM* 54: 117–128.

20. Bengough, G. D. 1912. A study of the properties of alloys at high temperatures. *Journal, Institute of Metals* 7: 123–174.

21. Mathew, M. D., Sasikala, G., Mannan, S. L., and Rodriguez, P. 1993. A comparative study of the creep rupture properties of Type 316 stainless steel base and weld metals. *Transactions of the ASME, Journal of Engineering Materials and Technology* 115: 163–170.

22. Hadrill, D. M., and Baker, R. G. 1965. Heat affected zone cracking in thick section austenitic steels during post weld heat treatment. *BWRA Bulletin* 6(11): 282–288.

23. Totsuka, N., Lunarska, E., Cragnolino, G., and Szklarska-Smialnowska, Z. 1987. *Corrosion* 43(8): 515–514.

24. Estman, J., Matsumoto, T., Narita, N., Heubaum, F., and Birnbaum, H. K. 1980. Hydrogen effects in nickel — Embrittlement or enhanced ductility. *Hydrogen Effects in Metals*, M. Bernstein and A. W. Thompson (eds.). Warrendale, Pa.: TMS pp. 397–409.

25. Symons, D. M. 1999. The effect of hydrogen in the fracture toughness of Alloy X-750 at elevated temperatures. *Journal of Nuclear Materials* 265: 225–231.

26. Huang, X., Zhang, Y., Liu, Y., and Hu, Z. 1997. Effect of small amount of nitrogen on carbide characteristics in unidirectional Ni-base superalloy. *Metallurgical Transactions A* 28(10): 2143–2147.

27. Palumbo, G., and Aust, K. T. 1992. Special properties of Σ grain boundaries. *Materials Interfaces — Atomic Level Structure and Properties*, Chapter 5. Great Britain: Chapman-Hall. pp. 190–211.

28. Bowers, R. 1997. Unpublished research. Edison Welding Institute, Columbus, Ohio.

29. Kikel, J. M., and Parker, D. M. 1998. Ductility dip cracking susceptibility of Filler Metal 52 and Alloy 690. *Proceedings of the Trends in Welding Research Conference*, Pine Mountain, Ga., pp. 757–762.

30. Pumphrey, P. H. 1976. Special high angle grain boundaries. *Grain Boundary Structure and Properties*, G. A. Chadwick and D. A. Smith, (eds.). London, U.K.: Academic Press, pp. 139–200.

31. Cordea, J. N., Evans, R. M., and Martin, D. C. 1962. Investigation to determine causes of fissuring in stainless steel and nickel-base alloy weld metals. *Technical Documentary Report No. ASD-TDR-62-317, Project No. 7381*, Task No. 738102. Columbus, Ohio: Battelle Memorial Institute. pp. 1–41.

32. Dix, A. W., and Savage, W. F. 1971. Factors influencing strain-age cracking in Inconel X-750. *Welding Journal* 51(6): 247-s to 252-s.

33. Zhang, Y., Nakagawa, H., and Matsuda, F. 1985. Weldability of Fe-36%Ni alloy (Report VI) — Further investigation on mechanism of reheat hot cracking in weld metal. *Transactions of JWRI* 14(2)

34. Zhang, Y., Nakagawa, H., and Matsuda, F. 1985. Weldability of Fe-36%Ni alloy (Report V) — Behaviors of grain boundary sliding and cavity formation preceding reheat hot cracking in weld metal. *Transactions of JWRI* 14(2): 119–124.

35. Unpublished data provided by J. Kikel of BWX Technologies, Inc., 2001.

36. Yeniscavich, W. 1966, A correlation of Ni-Cr-Fe alloy weld metal fissuring with hot ductility behavior. *Welding Journal* 45(8): 344-s to 355-s.